Impact of wave energy conversion on sediment transport

Brian Stiber, Asfaw Beyene

Department of Mechanical Engineering, San Diego State University, San Diego CA 92182,
abeyene@mail.sdsu.edu

Abstract

In this paper we examine the impact of wave energy conversion on sediment transport, - an important environmental consideration before the expected maturity of the technology. In order to accurately predict wave energy potential for sediment analysis, we solve the kW/m over the domain of interest for the entire calendar year using SWAN. We use a wind field input with six hour interval, 0.25° resolution from 6-satellite blended data from the National Climactic Data Center. Wave boundary conditions are obtained from three hour interval Wavewatch III hindcast data from the Marine Modelling and Analysis Branch of the Environmental Modelling Center of the National Center for Environmental Prediction. This is full discrete spectral data for all directions and frequencies from 0.0412 Hz to 0.406 Hz, for three points: 32.43°N -117.33°W, 32.63°N -117.44°W and 32.75°N -117.37°W. The bathymetric input was 3-arcsecond resolution Southern California Coastal Relief Model data obtained from the National Geophysical Data Center. Water level data is obtained from the National Ocean Service Center for Operational Oceanographic Products and Services for station number 9410230. The Coupled-Ocean-Atmosphere-Wave-Sediment Transport Model, aka COAWST was used to determine the erosion, suspension, transport and deposition of sediment. Coupling in COAWST is achieved using the Model Coupling Toolkit, MCT. The impact of wave farms on environmental conditions was then simulated, and found to be insignificant both in terms of effects on sediment deposition as well as changes in suspended sediment concentrations. In particular it was found that wave farms located in deep water where the wave resource is largest result in minimal harmful changes to coastal processes and the marine environment.

Keywords:

Wave energy, environmental impact, tool, renewable, Sustainability.

1. Wave energy

The vast energy quantity that can be harnessed, combined with the minor effect on the environment, make wave energy an appealing candidate for research and development. Currently, the small number of WEC configurations can only provide a partial representation of the environmental effects of such devices, [1], [2]. A unique benefit of wave energy is the seasonal fluctuation of power which mirrors the electricity requirement of temperate climates. The inconsequential land footprints and the movement to harness offshore wind energy also contribute to the advantages of wave power. Yet, the idea of wave energy conversion brings together important environmental, economic, social and ethical challenges, [1], [3].

Ocean waves are typically classified as wind waves and swell waves. Wind waves refer to waves created by local wind conditions. These waves have low periods and directions that vary little from that of the prevailing wind. Swell waves refer to waves with longer periods, which have propagated beyond the wind conditions where they originated. Sea states can include both wind and swell waves, and can be represented as a superposition of multiple wave trains each with their own period, significant height, and direction [4], [5]. When an unvarying wind exists over a fetch, eventually it will reach equilibrium with the sea state. This is referred to as a "fully developed" sea [5]. When this occurs, the energy distribution as a function of wave frequency, $S(f)$, is fit well by the empirical Pierson-Moskowitz spectrum [8]:

$$S(f) = \frac{\alpha g^2}{(2\pi f)^5} e^{-\beta\left(\frac{f_0}{f}\right)^4} \qquad (1)$$

where $\alpha = 8.1\text{x}10^{-3}$, $\beta = 0.74$, $f_0 = g/U_{19.5}$, and $U_{19.5}$ is the wind speed measured at 19.5m elevation.

In practice seas are never fully developed, and for this reason a modified Pierson Moskowitz spectrum called JONSWAP is often used. This spectrum has a narrower, higher band of peak frequencies, and is of the form [9]:

$$S(f) = \frac{\alpha g^2}{(2\pi f)^5} e^{-\frac{5}{4}\left(\frac{f_m}{f}\right)^4} \gamma^{e^{\left(\frac{-(f-f_m)^2}{2\sigma^2 f_m^2}\right)}} \qquad (2)$$

where the "Phillips constant" α = 0.076 $\tilde{x}^{-0.22}$, the nondimensional fetch $\tilde{x} = gx/U_{10}^2$, the peak frequency $f_m = 3.5\tilde{x}^{-0.33}$, $\gamma = 3.3$, and $\sigma = \begin{cases} 0.07 \text{ for } f \le f_m \\ 0.09 \text{ for } f > f_m \end{cases}$.

1.1. Wave resource

The total worldwide wave energy resource is estimated at about 1-10 TW [9] which is much lower than the 114,000 TW and 1,200 TW of solar and wind resource, respectively [10]. Wave power, however, has the advantage of a much higher power density than wind or solar – 2-3 kW/m^2 for wave energy as compared to 0.1-0.3 kW/m^2 for solar and 0.5 kW/m^2 for wind [5]. In addition, wave energy can be a more reliable renewable resource, available up to 24 hours a day as opposed to solar, and with more consistency and predictability than wind.

Individual waves are typically described using height or amplitude; period, frequency, or wavenumber; and direction. Sea states are the superposition of all the individual waves, and can have varying degrees of order, but are often analyzed as a stochastic process. Sea states vary with respect to location as well as time, with variations on all scales from hourly to seasonal. Lenee-Bluhm [6] et al have identified various papers describing wave resources across parts of Europe, North America and Australia. They studied the wave resource in the Pacific Northwest region of the US and found power density to increase up to sevenfold in the winter when compared to the summer. Wave amplitudes were higher, and the range in period was narrower during winter. The results illustrate the danger in underestimating extreme events based on a low average power, noting that a location with an average power density of 31 kW/m encountered a power of 200 kW/m at a rate of 1 occurrence per 100 events, associated with 1/10 of the yearly energy. From linear wave theory, the energy per unit area contained in a sea state is calculated as [5]:

$$\frac{E_{tot}}{A} = \frac{\rho g H_{m0}^2}{16} \qquad (3)$$

This energy consists of the gravitational potential and the kinetic energy associated with the fluid motion. The power transmission per unit length of wave crest is calculated as [5]:

$$\frac{P}{l} = c_g \frac{E_{tot}}{A} \qquad (4)$$

where c_g is the group velocity. In deep water $c_g = gT/4\pi$, therefore [5]:

$$\frac{P}{l} = \frac{\rho g^2 T H_{m0}^2}{64\pi} \qquad (5)$$

2. Modelling and analyses

Wave models describe the wind-induced creation and propagation of waves over domains of interest. Hydrodynamic models are used to study the interaction of WECs with the wave resource at the fluid-structure interface. Ocean models describe circulation and currents on various scales, as well as variations in temperature, salinity and density. Sediment models show the evolution of suspended and settled sediment matter, including seabed morphology. Other related geophysical models include ocean ice models, ocean biological and chemical models, and atmospheric models.

2.2. Wave modelling

Wave models are used to describe transfer of energy from wind, inter-wave interaction, bottom friction, shoaling and surf breaking, sea level setup and setdown, diffraction, vegetation based damping, wave-driven currents, and transmission, reflection, refraction and diffraction due to obstacles [11]. The foremost wave models in the coastal engineering industry are SWAN, the

"BW" wave module of MIKE 21, and the "S" or spectral version of REF/DIF [12]. SWAN is a phase averaging model based on an energy balance, REF/DIF S and MIKE 21 BW are phase resolved models based on potential flow analysis. REF/DIF (refraction/diffraction) solves the mild slope equation. Mike 21 BW solves the Boussinesq-type equation. SWAN solves the action balance equation. REF/DIF S is somewhat better for diffraction effects, but restricted in domain size, nonlinearity, direction, slope angle, and is monochromatic although different frequencies can be superimposed. MIKE 21 BW is better than REF/DIF for spectral interaction and dispersion, but is limited to long waves and by direction. SWAN is better for larger domains, nonlinearity and spectral applications and interactions as well as dispersion. SWAN is the only model of the three which can handle reflection, and most importantly wave generation and whitecapping from wind, but there are some issues with diffraction. SWAN has been chosen for this study because of its accessibility and adaptability as open source software, its native coupling with ocean models, its dominance in wave forecasting along with related third-generation models WAM and WAVEWATCH III [13], and its suitability for the relevant wave phenomena.

3. Ocean modelling

Ocean models are used to study the motion and state of seawater, its interaction with the atmosphere, and the transport of different types of materials in the oceans. The Earth's oceans comprise stratified fluids rotating with the planet beneath them. Their motion is caused by transfers of momentum and buoyancy, originated by forcing at the interface with the atmosphere. The Navier-Stokes equations relate this dynamically with good precision, representing many physical processes on numerous scales of time and space [14]. The majority of computational ocean models use an approximation to the Navier-Stokes equations, called the hydrostatic primitive equations, this approximation is so widespread within oceanographic modelling that it can be considered standard [14]. This approximation is appropriate for the large scale phenomena and northern latitudes considered in the present study [14].

Faithful modelling of ocean processes entails two principles, true representation of physical processes which have resolution at the time and space scales being used, as well as appropriate parametrization of sub-scale processes [15]. Three significant types of vertical coordinates have been traditionally used in ocean models, simple linear z-coordinates, ρ-coordinates based on potential density, and σ- coordinates, which are terrain (bathymetry) trackers. Each has advantages and disadvantages, and this selection is the most critical aspect of model construction [15]. In general, z-coordinates are well suited to the upper mixed layer, ρ-coordinates to the interior, and σ-coordinates to the bottom boundary layer (BBL). More recently an S-coordinate has been developed to enable high resolution in upper ocean layers for terrain-following σ-coordinates [16, 17]. The Regional Ocean Modelling System (ROMS, [17]) has been chosen for the present study due to its open and modular software, the diverse set of options available, an extensive community pursuing applications and providing support, the suitability of its S-type vertical coordinate, and the well-developed coupling capability with SWAN.

3.1. Modelling of WECs

Hydrodynamic modelling of wave energy converters has made use of software developed for studying the interaction of waves with vessels and offshore structures. Many different schemes have been studied using commercial panel method code such as WAMIT, which incorporates linear wave theory with a Boundary Element Method solver using source and doublet singularities [18, 19]. Another tool for modelling the hydrodynamics of marine structures is the OrcaFlex software, which is based on Finite Element Modelling using a lumped-mass analysis [20, 21]. Full Computational Fluid Dynamics (CFD) software can also be used to model hydrodynamic behavior [22]. These models can be useful for studying the performance of WECs under various conditions, but their use is outside the scope of this paper. Results of analyses using these models are available in the literature and have been used in the present study [18].

3.2. SWAN

In order to gain an understanding of the ocean energy potential, we use the SWAN [23, 24] software. Sea states are modeled as a superposition of many wave trains, and are described in terms of three bulk statistics: characteristic wave height, characteristic wave period and characteristic wave direction. The significant wave height used in SWAN is H_{m0}, and is equal to four times the square root of the sea surface height variance:

$$H_{m0} = 4\sqrt{\mathrm{VAR}(\zeta)} \quad (9)$$

where VAR is the variance function and ζ is the sea surface height. Using Equation (3) we have:

$$\frac{E_{tot}}{A} = \rho_0 g \mathrm{VAR}(\zeta) \quad (10)$$

The variance density spectrum (or spectral energy density), $G(f)$, is obtained by performing a Fourier transform on the autocovariance of sea surface height:

$$G(f) = 2\int_{-\infty}^{\infty} \mathrm{EV}(\zeta(t)\zeta(t-\tau))e^{-2\pi i f \tau} d\tau \quad (11)$$

for $f \geq 0$. EV is the expected value function. The variance spectrum density is so called because it has the property that:

$$\mathrm{VAR}(\zeta) = \int_0^{\infty} G(f) df \quad (12)$$

If ambient currents exist, spectral energy density is not a conservative property, therefore we introduce the spectral action density, $N(\sigma,\theta)$, which is conserved when currents exist and is defined as:

$$N = G/\sigma \quad (13)$$

The governing equation solved by SWAN is called the spectral action balance equation, and is expressed as:

$$\frac{\partial N}{\partial t} + \nabla_{\vec{x}} \cdot \left[\left(\vec{c}_g + \vec{U}\right)N\right] + \frac{\partial c_\sigma N}{\partial \sigma} + \frac{\partial c_\theta N}{\partial \theta} = S_{tot}/\sigma \quad (14)$$

The terms on the left describe the evolution of wave energy kinematically, with the second term representing the spatial propagation of wave energy, and the third and fourth terms describing the transport of wave energy in the spectral space. The wave energy forcing effects on the right side comprise an energy source term due to wind, source/sink nonlinear 3- and 4-wave interaction terms, and energy sink terms for dissipation due to whitecapping, bottom friction, and depth induced breaking. These terms include various empirical formulations, with whitecapping related to the ratio of wave height to wavelength, and breaking related to the ratio of wave height to bottom depth. The action balance equation is discretized using the Finite Difference method, and solved using Gauss-Seidel iteration. SWAN is referred to as a third-generation wave model, this is defined by it treatment of the source and sink term parametrizations [13].

The n-th moment of the variance density spectrum,

$$m_n = \int_0^{\infty} f^n G(f) df \quad (15)$$

is used to define various parameters – Equation (15) for example shows that the variance is equal to the 0^{th} moment, and this moment is the basis for the significant wave height used by SWAN:

$$H_{m0} = 4\sqrt{m_0} \quad (16)$$

Different moments can also be combined to express various forms of the characteristic wave period.

$$T_{m-10} = m_{-1}/m_0 \quad (17)$$

3.3. COAWEST

In order to study the processes involved in the erosion, suspension, transport and deposition of sediment, we use the Coupled-Ocean-Atmosphere-Wave-Sediment Transport Model, or COAWST [25, 26]. This model comprises the ROMS ocean model, the Weather Research and Forecasting (WRF) atmospheric model, the SWAN wave model, and the Community Sediment Transport

Model (CSTM) sediment model. The atmospheric model was not used in this study, instead the option of providing surface fluxes, forcing and boundary conditions via bulk parameters was used. COAWST enables two-way coupling between ROMS and SWAN with variables being transferred between the two models at user-defined time steps. The size of these time steps must be an integer multiple of each of the time steps used in the individual wave and ocean models.

To evaluate the impacts of WECs on the wave field over the domain and by extension the impacts on sediment conditions, we first use the COAWST software to model the domain in the absence of WECs. We then alter the SWAN wave model portion of the software to simulate a reduction in wave energy due to WECs. This altered wave model is coupled with the ocean and sediment model using COAWST to evaluate the effects of WECs on sediment conditions.

3.3.1. ROMS

The ocean circulation model used in COAWST is ROMS [16, 17]. ROMS is a class of 3D, free-surface, terrain-following numerical model that solves the Reynolds-averaged Navier-Stokes equations using the hydrostatic and Boussinesq assumptions. The ROMS model uses atmospheric inputs including air temperature, pressure and humidity, surface radiation and other heat fluxes, wind speed or stress, evaporation and precipitation. Boundary conditions include water level, momentum, salinity and temperature.

ROMS solves the governing primitive equations – a formulation of the conservation of momentum, the advection-diffusion equation, the equation of state for seawater, and the continuity equation. The Reynolds-averaged formulation of the horizontal momentum equations in Cartesian coordinates are given by:

$$\frac{\partial U}{\partial t} + \vec{V} \cdot \nabla U - fV = -\frac{\partial \phi}{\partial x} - \frac{\partial}{\partial z}\left(\overline{U'W'} - \nu \frac{\partial U}{\partial z}\right) + F_U + D_U \qquad (18)$$

$$\frac{\partial V}{\partial t} + \vec{V} \cdot \nabla V - fU = -\frac{\partial \phi}{\partial y} - \frac{\partial}{\partial z}\left(\overline{V'W'} - \nu \frac{\partial V}{\partial z}\right) + F_V + D_V \qquad (19)$$

The prime notation indicates a variation around the mean, the overbar indicates an average over time. The hydrostatic assumption gives as a force balance in the vertical dimension:

$$\frac{\partial \phi}{\partial z} = \frac{-\rho g}{\rho_0} \qquad (20)$$

Note that variations in density are significant and accounted for in this equation where the density is multiplied by the acceleration of gravity, g, in the buoyancy term. These variations are neglected elsewhere in the momentum equations due to the Boussinesq approximation. Conservation of mass for an incompressible fluid is given by:

$$\frac{\partial U}{\partial x} + \frac{\partial V}{\partial y} + \frac{\partial W}{\partial z} = 0 \qquad (21)$$

The equation of state for seawater is expressed as:

$$\rho = \rho(T, S, P) \qquad (22)$$

The nonlinear equation of state used in this study is based on the UNESCO EOS-80 formulation and was developed to compute the density *in situ* from potential temperature, salinity and pressure [27]. Transport of tracer type variables are governed by the advection-diffusion equation:

$$\frac{\partial C}{\partial t} + \vec{V} \cdot \nabla C = -\frac{\partial}{\partial z}\left(\overline{C'W'} - \nu_\theta \frac{\partial C}{\partial z}\right) + F_C + D_C \qquad (23)$$

ROMS is discretized horizontally onto an orthogonal curvilinear grid. The Arakawa-C grid used with grid coordinates ξ and η [28]. Density, temperature, salinity and sea surface height are prescribed at ρ-points in the centers of cells velocities are prescribed at cell edges. ψ-points define grid cell nodes. Boundary conditions are given by values on and outside the outer edges.

3.3.2. Sediment model

Sediment can be accounted for in ROMS using options based on the CSTM software. The model is initialized with a user-defined number of bed layers having user-defined thicknesses. The user also defines a changeable number of sediment classes, each class having defined characteristics such as

grain size, porosity, etc. When the critical shear stress is exceeded at the bottom boundary, erosion occurs. When the shear stress drops below a user-defined threshold, deposition occurs. New layers are formed when deposited material exceeds a user-defined thickness. The number of layers is held constant by merging or dividing the bottom layer as necessary. A depiction of the model processes is shown in *Figure 1*, [26]. The model is capable of handling both cohesive and non-cohesive sediment types (mud and sand). Important user inputs include the thickness required to create a new layer, initial bed conditions, as well as median grain diameter, suspended sediment concentration, grain density, settling velocity, erosion rate, critical shear stress, and porosity for each sediment class.

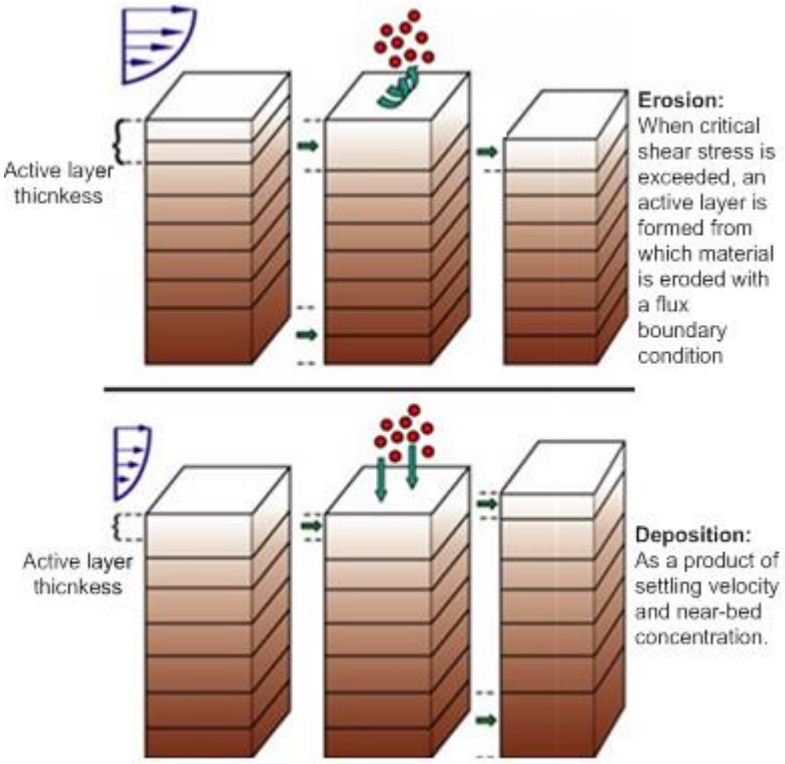

Figure 1.CSTM sediment model, adopted from [26]

3.3.3. Model coupling

Coupling in COAWST is achieved using the Model Coupling Toolkit (MCT). MCT is a parallel software protocol using message passing interfaces to facilitate two-way coupling between ROMS and SWAN. MCT handles the allocation of processors, transfer of data between models, and interpolation of transferred data fields. A schematic of the model coupling with transferred data types is shown in *Figure 2*.

3.4. Model description

In order to accurately predict wave energy potential, we solve over the entire domain of interest and average over the entire calendar year of 2010. The wind field input used was six hour interval, 0.25° resolution, 6-satellite blended data from the National Climactic Data Center (NCDC). This data required a small amount of interpolation. Wave boundary conditions are obtained from three hour interval Wavewatch III hindcast data from the Marine Modelling and Analysis Branch (MMAB) of the Environmental Modelling Center (EMC) of the National Center for Environmental Prediction (NCEP). This is full discrete spectral data for all directions and frequencies from 0.0412 Hz to 0.406 Hz, for three points: 32.43°N -117.33°W, 32.63°N -117.44°W and 32.75°N -117.37°W. The bathymetric data is 3-arcsecond resolution Southern California Coastal Relief Model data obtained from the National Geophysical Data Center (NGDC). Water level data is obtained from the National Ocean Service (NOS) Center for Operational Oceanographic Products and Services

(CO-OPS) for station number 9410230. The resulting system was simulated on a laptop equipped with an Intel Core 2 Duo T6500 processor with 4GB of RAM, utilizing a grid resolution of 20x22. With a time step value of 3 hours, the entire simulation required around 30 hours of CPU time.

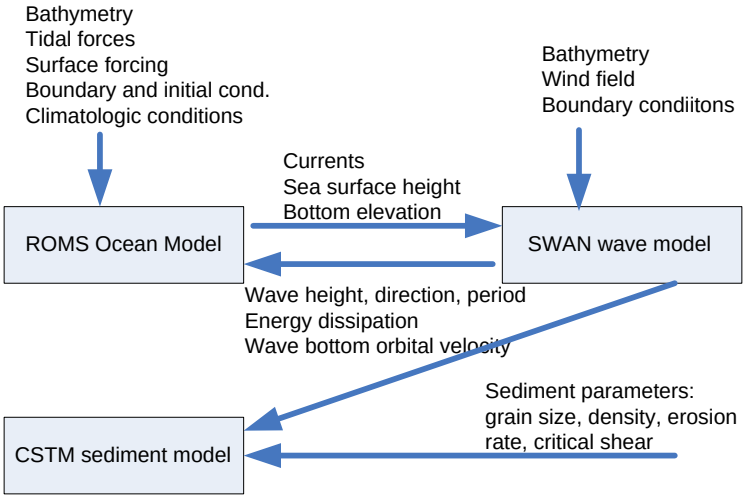

Figure 2. Schematic of model coupling

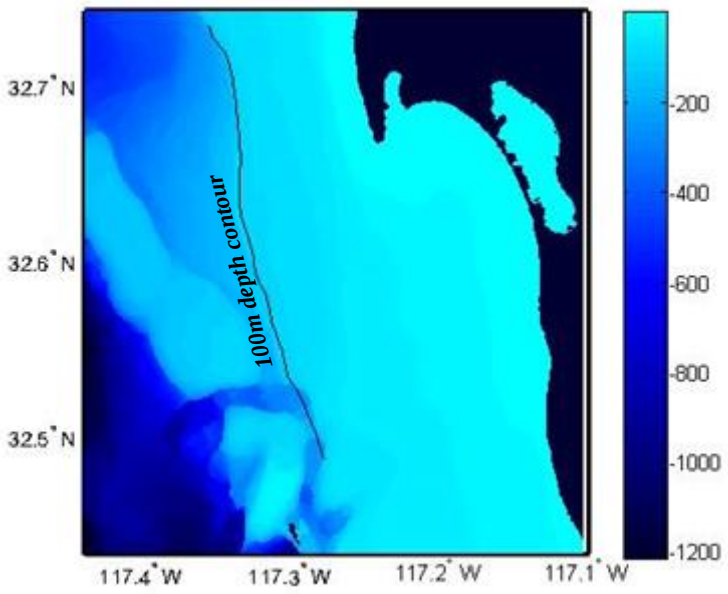

Figure 3. Bathymetric (depth) data of the domain under consideration

SWAN can calculate and output various bulk parameter data such as H_{mo}, P/l, and various forms of characteristic period and direction, as well as spectral data $G(\sigma,\theta)$, at user selected points. To sum up the resource we perform a line integral on the total energy transport across the 100m contour. Thirty-four points, equally spaced between 32.48°N and 32.74°N are sampled, and the annual average wave power per unit crest length across each of the i=33 line segments is calculated as:

$$\frac{P}{l}_{avg,i} = \frac{1}{2920}\sum_{n=1}^{2920}\left(\left(\frac{P}{l}\right)_{i,n} + \left(\frac{P}{l}\right)_{i+1,n}\right)/2 \qquad (24)$$

where i is the index of line segments, from 1 to 33, and n is the time step of each run, from 1 to 2,920. The total average power across each line segment is found by multiplying by the line segment length, s_i:

$$P_{avg,i} = s_i \frac{P}{l_{avg,i}} \qquad (25)$$

The WEC efficiencies, the wave farm density, and the SECs to single values have been condensed to single values rather than a set of various values for different conditions. This is because of the lack of validated data for varying operating conditions.

4. Results and conclusion

SWAN output was generated for a grid coincident with the computational and bathymetric grids, as well as along a 100m depth contour line. To show the annual variation in H_{m0}, we chose one point of interest along the 100m depth contour, at 32.69°N 117.34°W, and present the SWAN output for significant wave height at that point throughout the year. *Figure 4* shows the annual local total wave power per meter of wave crest.

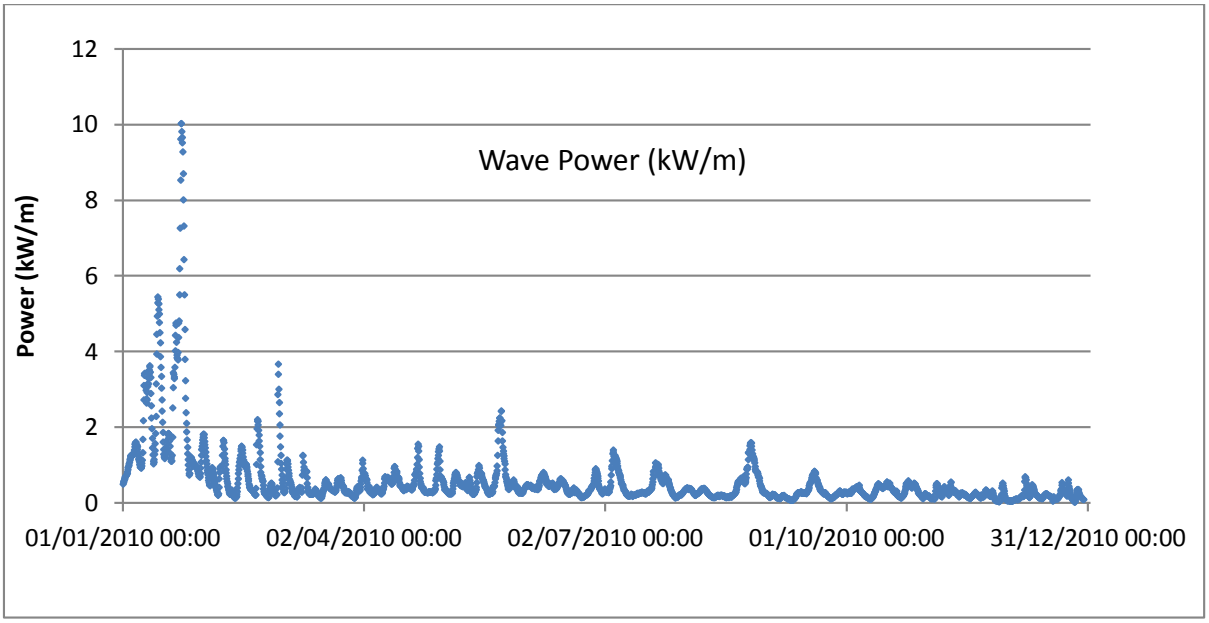

Figure 4. Wave energy over the calendar year 2010 at 32.69°W 117.34°W.

After running the COAWST model over both the larger and nested domains for the selected time period, the changes in calculated wave heights, sediment bed thicknesses, water column sediment concentrations, energy density and bottom wave orbital velocity were calculated by comparing the calculated parameters obtained from the nested run with wave energy removed, with those obtained in the original run. Figure 5 shows the difference in significant wave height, in meters, for the nested subdomain at the 550th time step. The effect of removing the energy along the western boundary can be seen clearly in the two grid cells which represent the location of the WECs. Note also that the difference decreases rapidly with distance from the WEC location.

Figure 6 shows the difference in sediment bed thickness, measured in meters, for the 550^{h}, 1100th, and 1650th time steps. Overall, the effect of the WECs on the sediment bed environment is seen to be quite small. It is notable that there is sediment deposition that occurs with the wave farm in areas where it did not occur without WECs.

Figure 7 shows the difference in net sediment deposition at the 550th, 1100th, and 1650th time steps, in meters, at grid points with j indices equal to 29 along the η-direction. This plot shows a slight increase in sediment deposition near the WEC location, as well as a slight decrease in the shoreward direction. As we approach the surf zone deposition changes to erosion, with decreased erosion in the wave. The vertical cross section shown is for the row with index j=29 in the η-direction.

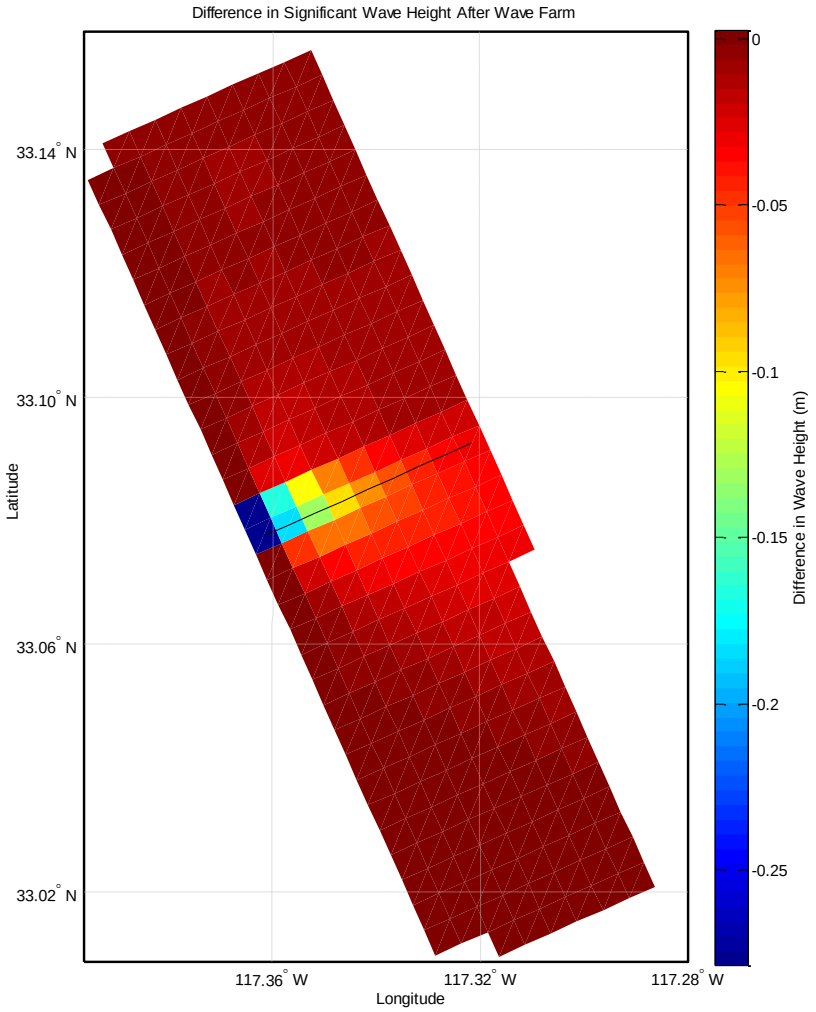

Figure 5. Difference in wave height over nested domain after wave farm

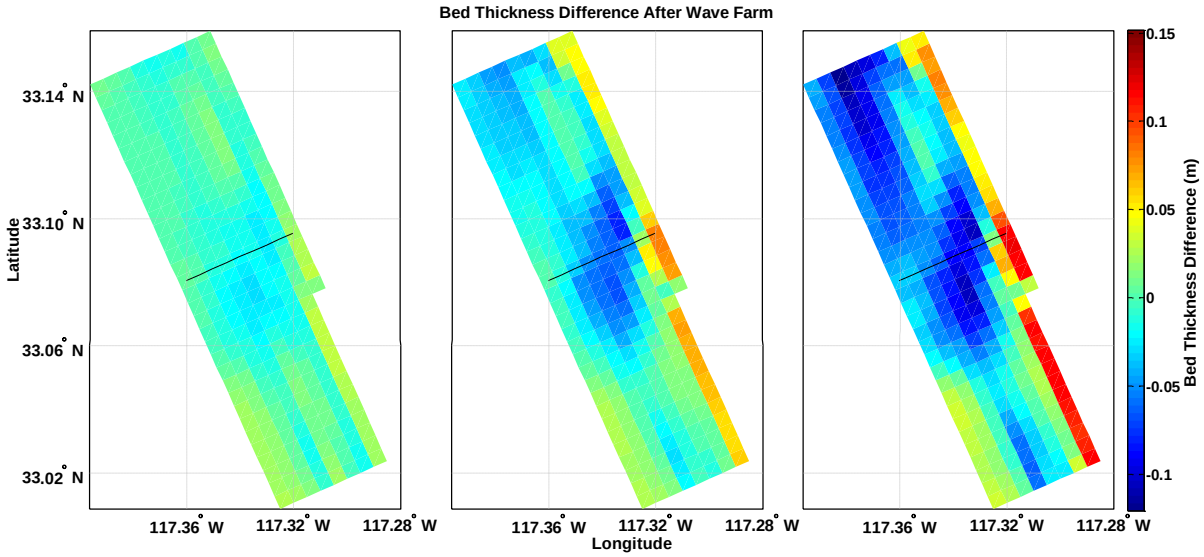

Figure 6. Difference in sediment bed thickness after wave farm

The y-axis of the plot is the depth given in meters, and the x-axis is the longitude in degrees east. The plot also shows that the change in sediment concentration due to WECs is confined to the lowest levels of the water column. In general one can see that the effect of the wave farm on the suspended sediment environment is very small.

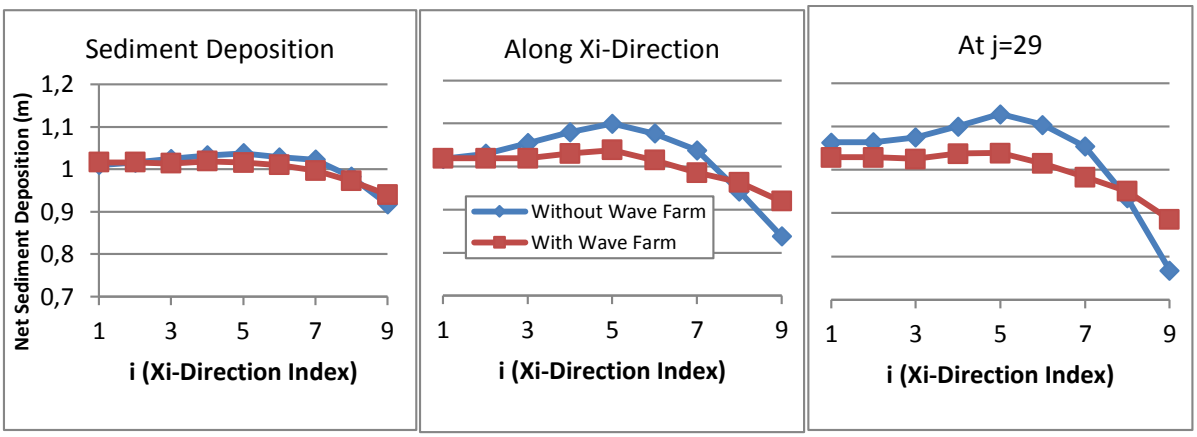

Figure 7. Sediment deposition before and after wave farm

In conclusion, we examined the impact of WECs on sediment transport. SWAN software was used to simulate the wave climate for a calendar year using input data from several sources. The impact of wave farms on environmental conditions was found to be insignificant, both in terms of effects on sediment deposition as well as changes in suspended sediment concentrations. In particular it was found that wave farms located in deep water where the wave resource is largest result in minimal harmful changes to coastal processes and the marine environment.

Nomenclature

c_σ, c_θ	wave propagation in spectral space
$c, \vec{c}_g$	group velocity, m/s
C	tracer type variable, e.g. temperature, salinity, sediment concentration
d	water depth, m
D_U, D_V, D_C,	horizontal diffusion terms
E_{tot}/A	total energy per unit surface area, J/m^2
f	frequency, Hz
f_m	peak frequency, Hz
$f(x,y)$	Coriolis parameter
F	wave farm density, %
F_U, F_V, F_C,	ROMS forcing terms
g	gravitational acceleration, 9.81 m/s^2
$G(f, \theta)$	variance density spectrum(energy density spectrum), m^2/Hz-radian
h	sea floor depth (relative to datum height), m
H_{m0}	significant wave height
i	ROMS grid ξ-direction index
j	ROMS grid η-direction index
k	wavenumber, radians/m
L	ROMS grid ξ-direction index maximum
L_m	ROMS grid ξ-direction index interior maximum
M	ROMS grid η -direction index maximum
M_m	ROMS grid η -direction index interior maximum
$N(f,\theta)$	action density spectrum
P/l	power per unit length, kW/m
P	total pressure
r_{CW}	capture width ratio, unitless
S	wave energy source/sink term
S	salinity, P.S.U.
$S(f)$	wave energy spectrum
t	time
T	wave period, s
T	potential temperature, K
U_{10}	wind speed at 10m height
$U_{19.5}$	wind speed at 19.5m height
U,V,W	current velocity components, m/s
W_C	capture width, m
$\vec{V}$	current velocity vector, m/s (U,V,W)
$\tilde{x}$	nondimensional fetch length
x,y,z	cartesian coordinates, m

Greek symbols

α	Phillips constant
γ	JONSWAP peak enhancement parameter
ζ	sea surface height, m
η	ROMS Arakawa-C grid local coordinate
η_{WEC}	wave converter efficiency
θ	direction
λ	wavelength, m
ν	viscosity
ξ	ROMS Arakawa-C grid local coordinate
ρ_0	seawater density, 1025 kg/m^3
$\rho_0 + \rho(x,y,z,t)$	total density calculated *in situ* by ROMS
σ	relative frequency(radians/s)
ϕ	dynamic pressure, $\phi=P/\rho_0$
ω	absolute frequency(radians/s)

References

[1] A. Clément, P. McCullen, A. Falcão, A. Fiorentino, F. Gardner, K. Hammarlund, G. Lemonis, T. Lewis, K. Nielsen, S. Petroncini, M.-T. Pontes, P. Schild, B.-O. Sjöström, H. C. Sørensen and T. Thorpe, "Wave energy in Europe: current status and perspectives," *Renewable and Sustainable Energy Reviews,* vol. 6, pp. 405-431, 2002.

[2] A. Beyene and J. H. Wilson, "Comparison of wave energy flux for northern, central, and southern coast of California based on long-term statistical wave data," *Energy,* pp. 1856-1869, 2006.

[3] A. Beyene and J. Wilson, "Digital mapping of California wave energy resource," *International Journal of Energy Research,* pp. 1156-1168, 2007.

[4] A. Beyene and J. H. Wilson, "Parameter Variation and Part-Load Efficiencies of Wave Energy Conversion," *Journal of Energy Engineering,* pp. 15-26, 2006.

[5] J. Falnes, "A review of wave-energy extraction," *Marine Structures,* vol. 20, pp. 185-201, 2007.

[6] W. J. J. Pierson and L. A. Moskowitz, "Proposed Spectral Form for Fully Developed Wind Seas Based on the Similarity Theory of S. A. Kitaigorodskii," *Journal of Geophysical Research,* vol. 69, pp. 5181-5190, 1964.

[7] K. Hasselmann, T. Barnett, E. Bouws, H. Carlson, D. Cartwright, K. Enke, J. Ewing, H. Gienapp, D. Hasselmann, P. Kruseman, A. Meerburg, P. Mller, D. Olbers, K. Richter, W. Sell and H. Walden, "Measurements of wind-wave growth and swell decay during the Joint North Sea Wave Project (JONSWAP)," *Ergnzungsheft zur Deutschen Hydrographischen Zeitschrift Reihe,* pp. 1-95, 1973.

[8] P. Davies, "Wave-powered desalination: resource assessment and review of technology.," *Desalination,* vol. 186, pp. 97-109, 2005.

[9] P. Lenee-Bluhm, R. Paasch and H. T. Özkan-Haller, "Characterizing the wave energy resource of the US Pacific Northwest," *Renewable Energy,* pp. 2106-2119, 2011.

[10] The SWAN Team, "SWAN User Manual," 2013.

[11] S.-H. Oh, K.-D. Suh, S. Y. Son and D. Y. Lee, "Performance Comparison of Spectral Wave Models Based on Different Governing Equations Including Wave Breaking," *KSCE Journal of Civil Engineering,* vol. 13, pp. 75-84, 2009.

[12] R. Jensen, P. Wittmann and J. Dykes, "Global and regional wave modeling activities," *Oceanography,* vol. 15, pp. 57-66, 2002.

[13] J. Marshall, C. Hill, L. Perelman and A. Adcroft, "Hydrostatic, quasi-hydrostatic, and nonhydrostatic ocean modeling," *Journal of Geophysical Research,* vol. 102, pp. 5733-5752, 1997.

[14] S. M. Griffies, C. Böning, F. O. Bryan, E. P. Chassignet, R. Gerdes, H. Hasumi, A. Hirst, A.-M. Treguier and D. Webb, "Developments in ocean climate modelling," *Ocean Modelling,* vol. 2, pp. 123-192, 2000.

[15] Y. Song and D. Haidvogel, "A semi-implicit ocean circulation model using a generalized topography-following coordinate system," *Journal of Computational Physics,* vol. 115, pp. 228-244, 1994.

[16] A. F. Shchepetkin and J. C. McWilliams, "The regional oceanic modeling system (ROMS): a split-explicit, free-surface, topography-following-coordinate oceanic model," *Ocean Modelling,* vol. 9, pp. 347-404, 2005.

[17] A. Babarit, J. Hals, M. Muliawan, A. Kurniawan, T. Moan and J. Krokstad, "Numerical

benchmarking study of a selection of wave energy converters," *Renewable Energy,* vol. 41, pp. 44-63, 2012.

[18] R. Gomes, J. Henriques, L. Gato and A. Falcão, "Hydrodynamic optimization of an axisymmetric floating oscillating water column for wave energy conversion," *Renewable Energy*, vol. 44, pp. 328-339, 2012.

[19] X. Chena, J. Zhang, P. Johnson and M. Irani, "Dynamic analysis of mooring lines with inserted springs," *Applied Ocean Research,* vol. 23, pp. 277-284, 2001.

[20] V. Krivtsov and B. Linfoot, "Disruption to benthic habitats by moorings of wave energy installations: A modelling case study and implications for overall ecosystem functioning," *Ecological Modelling,* vol. 245, pp. 121-124, 2012.

[21] E. B. Agamloh, A. K. Wallace and A. v. Jouanne, "Application of fluid–structure interaction simulation of an ocean wave energy extraction device," *Renewable Energy,* vol. 33, pp. 748-757, 2008.

[22] SWAN (Simulating WAves Nearshore); a third generation wave model. Copyright © 1993-2013 Delft University of Technology, 2013.

[23] The SWAN Team, "SWAN Scientific and Technical Manual," 2013.

[24] J. C. Warner, B. Armstrong, R. He and J. B. Zambon, "Development of a Coupled Ocean–Atmosphere–Wave–Sediment Transport (COAWST) Modeling System," *Ocean Modelling,* vol. 35, pp. 230-244, 2010.

[25] J. C. Warner, C. R. Sherwood, R. P. Signell, C. K. Harris and H. G. Arango, "Development of a three-dimensional, regional, coupled wave, current, and sediment-transport model," *Computers & Geosciences,* vol. 34, pp. 1284-1306, 2008.

[26] D. R. Jackett and T. McDougall, "Minimal Adjustment of Hydrostatic Profiles to Achieve Static Stability," *Journal of Atmospheric and Oceanic Technology*, vol. 12, pp. 381-389, 1995.

[27] K. S. Hedström, *DRAFT Technical Manual for a Coupled Sea-Ice/Ocean Circulation Model (Version 4),* 2012.